A study on the Characteristics of In-Cylinder Intake Flow in Spark Ignition Engine Using the PIV

Suk-Young Lee

Department of Mechanical Engineering, Pusan National University,
30 Jangjeon-dong, Geumjeong-gu, Busan 609-735, Korea

Ku-Seob Jeong

Department of Automotive Engineering, jinju International University,
270 Sangmoonri, Moonsaneub, Jinju city, Kuyungsang-namdo 609-735, Korea

Chung-Hwan Jeon*

Department of Mechanical Engineering, Pusan National University,
30 Jangjeon-dong, Geumjeong-gu, Busan 609-735, Korea

Young-June Chang

Department of Mechanical Engineering, Pusan National University,
30 Jangjeon-dong, Geumjeong-gu, Busan 609-735, Korea

In this study, to investigate in-cylinder tumble or swirl intake flow of a gasoline engine, the flow characteristics were examined with opening control valve (OCV) and several swirl control valves (SCV) which intensify intake flow through steady flow experiment, and also turbulent characteristics of in-cylinder flow field were investigated by 2-frame cross-correlation particle image velocimetry (PIV) method. In the investigation of intake turbulent characteristics using PIV method, the different flow characteristics were showed according to OCV or SCV figures. The OCV or SCV installed engine had higher vorticity and turbulent kinetic energy than a baseline engine, especially around the wall and lower part of the cylinder. Above all, SCV B type was superior to the others. About energy dissipation and reynolds shear stress distribution, a baseline engine had larger loss than OCV or SCV installed one because flow impinged on the cylinder wall. It should be concluded, from what has been said above, as swirl component was added to existing tumble flow adequately, it was confirmed that turbulent intensity was enlarged, flow energy was conserved effectively through the experiment. In other words, there is a suggestion that flow characteristics as these affected to in-cylinder combustion positively.

Key Words : Particle Image Velocimetry, Cross Correlation, Swirl Control Valve, Open Control Valve, Flow Visualization

1. Introduction

An important factor in the configuration of the intake ports and the combustion chamber is,

* Corresponding Author,
  E-mail : chjeon@pusan.ac.kr
  TEL : +82-51-510-3035; **FAX** : +82-51-510-9818
  Department of Mechanical Engineering, Pusan National University, 30 Jangjeon-dong, Geumjeong-gu, Busan 609-735, Korea. (Manuscript **Received** June 30, 2004; **Revised** December 15, 2004)

in addition to the vaporization characteristics of the fuel, the formation of flow fields within the vehicle's engine. It has been reported that the flow field around the flame during flame propagation in an SI engine is a determining factor in the combustion process, ie greatly affecting heat efficiency, engine performance, and emissions reduction (Hacohen et al., 1994). In this regard, a detailed analysis of the flow characteristics in the cylinder is necessary to devise a combustion acceleration method. Due to its mechanical con-

figuration, the commonly used pentroof combustion chamber has an advantage in generating tumble flows as opposed to swirl flows. Many researchers have attempted to increase combustion efficiency by studying tumble flows : First, the spatial velocity distribution of the tumble flow field formation during intial intake is analyzed quantitatively. Second, the results are used in designing the intake ports and the combustion chamber. Finally, the turbulence generation process is analyzed (Ronnback et al., 1991).

Until recently, research concentrated upon turbulence flow field measurements, which were conducted using Hot Wire Anemometry (HWA) and Laser Doppler Velocimetry (LDV) to measure the mean and fluctuation velocity component. This method, however, is a point measurement method, and is not appropriate for analyzing spatial flow field patterns. An actively developing field for such studies is the Particle Image Velocimetry (PIV), which uses optical equipment, such as lasers, and computer-based digital imagery. The PIV system not only has many advantages of the LDV, but can be used for comprehensively analyzing non-steady state flows, as well as quantitatively and qualitatively measuring spatial change ; thus, PIV is appropriate for flow measurements within the engine cylinder (Lee et al., 1993). The current research employs a steady-state flow experiment apparatus and PIV apparatus to measure the flow characteristics in a cylinder of a commercial pentroof gasoline engine. Specifically, the research focused on the in-cylinder flow characteristics when intake port configuration is changed, affecting the tumble flow, and changing results from different opening control valve (OCV) or swirl control valve (SCV) configurations. A 2-frame cross-correlation PIV technique was used to visualize the turbulence-creation process within the combustion chamber during intake flow field intensification. Furthermore, speed, vorticity, flow intensity, turbulence intensity, energy loss, and other turbulence-specific factors were examined qualitatively and quantitatively. These were contrasted with the flow fields of baseline gasoline engines that were not affected by flow field inten-

sification.

2. Experimental Setup and Methodology

2.1 Experimental apparatus and conditions

Figure 1 show steady-state flow experimental apparatus which is to measure the flux, swirl, and tumble intensity. To measure intake flow, a laminar flow meter was installed, and the differential pressure was gauged by micro-manometer from 1 to 1000 mmH$_2$O. The experiment was operated with acrylic tumble adapter attached to measure tumble and swirl intensity. The steady-state experimental apparatus was used to determine the changes in the intake flux, swirl, and tumble intensity for each OCV or SCV. In the experiment, the valve lift was operated from 0 to 8 mm by 1 mm, and to measure intake flow, flow coefficient was calculated by pressure valve of laminar flow meter. In-cylinder swirl and tumble intensity were represented by non-dimensional rig swirl or tumble by using tumble adapter. NRS and NRT are defined by angular velocity of paddle wheel as seen below.

$$NRS \text{ or } NRT = \frac{w_p B}{v_0} \qquad (1)$$

where

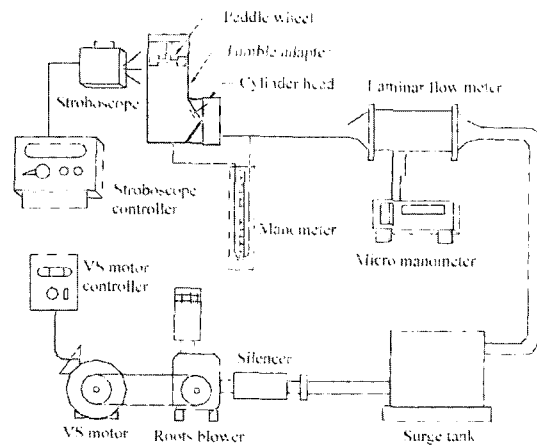$$v_0 = \left[\frac{2(p_0 - p_c)}{\rho} \right]^{1/2}$$

Fig. 1 Schematic diagram of experimental apparatus

B represents the cylinder bore, ω_p the paddle angular velocity, v_o the characteristic velocity, and p_o and p_c represents intake and in-cylinder pressure respectively.

Figures 2 and 3 show schematic diagrams of the PIV measurement system and gasoline engine steady-state flow experimental apparatus. The PIV system in the current research was composed of a dual-pulse Hd : Yag laser system with energy of 200 mJ and wavelength of 532 nm ; a $1K \times 1K$ high-resolution CCD camera (PIVCAM 10-15), synchronous apparatus (TSI 610032) and a driving pentium computer for image processing. A Nikon 50 mm standard-lens was attached to the CCD camera to minimize image distortion errors, and the time intervals between frames were set at a maximum of 35 μs in order to measure high-speed flows. The laser beam was projected

through a cylindrical lens to create a laser sheet for use in the flow analysis, and the CCD camera was set up perpendicularly to the laser sheet for obtaining the particle images. The steady-state flow experimental apparatus employed a blower for air inflow. The blower specifications were maximum pressure of 1.2 atm, output of 7.5 kW, and flow of 5.6 m³/min. Pressure differences between the front and behind laminar flow meters, that are installed to measure intake flow, were measured in the range of $1 \sim 1000$ mmH₂O with a micro-manometer. Furthermore, the pressure difference between the multi intake port ·and in-cylinder was maintained at a constant 250 mmH₂O during the experiment. The cylinder head used in the research was a pentroof, 2000 cc, with an acrylic tumble adapter attached to the first cylinder to facilitate measurements. The tumble adapter was 5 mm thick and had an inner diameter of 85 mm which is identical to the cylinder diameter. Laskin nozzles, which use the principle of cavitation, were used to produce olive oil aerosol. The aerosol was used as tracking particles in this research with an average diameter of 2 μm, and it was appropriate for use in PIV of fluid flows (Melling, 1997). Table 1 shows the experimental conditions for the OCV, SCV and intake valve lifts that were used when examining flow aspects. The OCV or SCV configurations and open ratios were selected as shown in Fig. 4
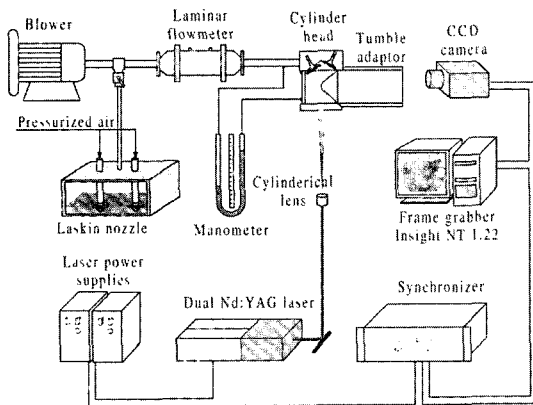

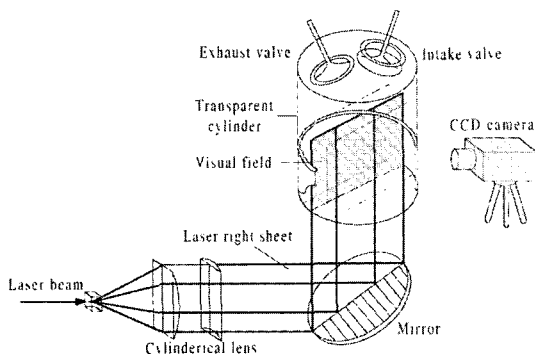Fig. 2   Schematic diagram of experimental apparatus

Fig. 3   Schematic diagram of experimental apparatus for the side view in the vertical cutting plane

Table 1   Experimental conditions

Visual field	Cylinder center			
SCV types	Baseline	OCV A	SCV B	SCV C
Open ratio (%)	100	89	72.5	78
Valve lift (mm)	2, 4, 6, 8			
Interval of 2 frames	$\Delta t \geq 35$ μs			

OCV A   SCV B   SCV C
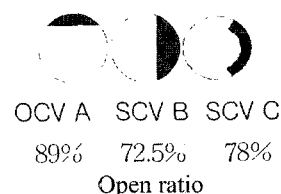
89%   72.5%   78%

Open ratio

Fig. 4   Configurations of OCV and SCV

to minimize the flux coefficient loss while maximizing the swirl intensity. Furthermore, the intake valve lift was increased at 2 mm intervals from 2 to 8 mm, and the flow field was measured to find and compare the turbulent characteristics.

### 2.2 Velocity vector calculation and post-processing

The algorithm used to obtain velocity vectors was the 2-frame cross-correlation technique. For the velocity vector, there are $6400(80\times80)$ lattice number and the spatial resolution between vectors is 0.93 mm. The true length of one pixel is 0.096 mm, and software inaccuracies occur during sub-pixel tracking as a result of image resolution limitations. The interrogation region for finding the maximum cross-correlation coefficient is 24×24 pixels in size. The true size of the interrogation region is approximately 2.304 mm, with a 50% overlap allowance. The velocity vectors obtained through the above technique were processed through the PIV ACE 1.0 processing program for post-processing such as validating faulty vectors ; centroid track ; ensemble averaging ; and interpolation, as well as for obtaining statis -ical measures. The pre-process velocity vectors were validated, and discarded if necessary, by comparing the absolute values of the u, v vector ; size as compared to surrounding vectors ; differences in direction ; etc. To substitute the removed vectors, Gaussian weighting function was used : eight vectors surrounding the removed vector are used to find an approximate value. This was followed by a process where the vector values are converted from pixel units to actual velocity vector units (m/s), and the velocity vector were extracted. 510 instances of velocity fields were obtained from 1020 images, and these were ensemblely averaged to obtain the mean flow field.
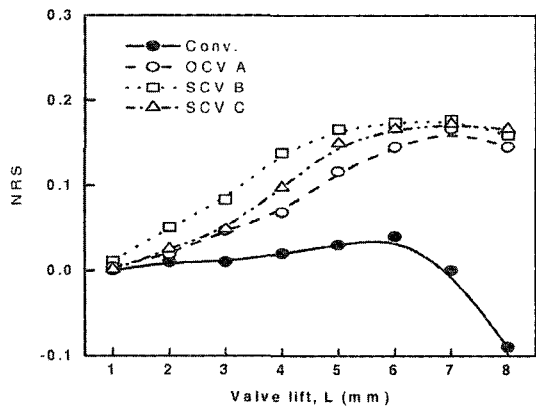
3. Results and Analysis

3.1 Steady-state flow characteristics according to OCV and SCV configurations

Through steady-state flow experiment, three different shapes of OCV and SCV were selected.
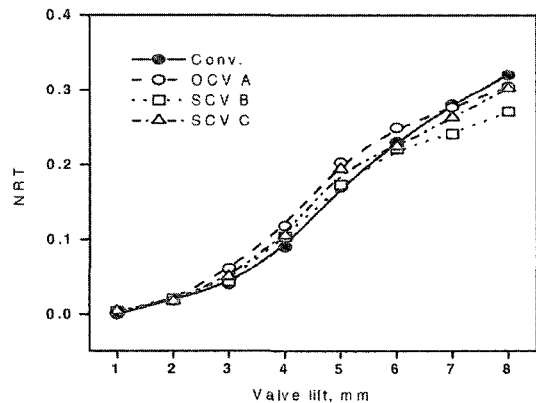
Flux coefficient, NRS and NRT were measured and the result is displayed in Figs. 5, 6 and 7.
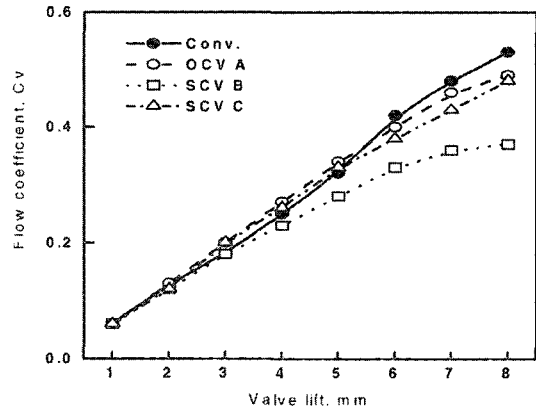
Fig. 5 Effects of OCV and SCV configuration of flow coefficient

Fig. 6 Effects of OCV and SCV configuration on non dimensional rig swirl

Fig. 7 Effects of OCV and SCV configuration on non dimensional rig tumble

Figure 5 shows change of flux coefficient according to valve lift. Installation of OCV or SCV turns to be an obstacle and to diminish Cv. And OCV A which has the biggest open ratio has shown the biggest Cv, SCV which has the smallest open ratio to have the smallest Cv. Figures 6 and 7 shows the intensity of NRS and NRT. The absolute value of NRS is augmented by installation of OCV or SCV, and SCV B is revealed to have the higher grade of swirl than any others. While swirl that generated in former engine tend to reverse in swirl direction according to the increment of valve lift. And swirl that generated in OCV or SCV-installed engine tends to have fixed direction. Looking over NRT, it does not appear to have a serious difference whether SCV is installed or not. But looking over NRS, it appears to decrease in order of OCV A, SCV C, SCV B. On the basis of these experiment, flow angle can be defined by ratio of NRT to NRS as written below, and the result is shown on Fig. 8 (Arcoumanis et al., 1993). It is shown on Table 2 that calculated Ricardo swirl ratio using valve lift curve.

$$\theta_f = \tan^{-1}\left(\frac{NRT}{NRS}\right) \qquad (2)$$

As seen on Fig. 8, in case of the former engine without OCV or SCV, flow angle is about 80 degree and tumble flow is dominant over swirl flow. Installing OCV or SCV, swirl flow has been reinforced. and flow angle maintains around 40-60 degree even under the condition that valve lift is 8 mm. Following Furuno's study (Furuno et al., 1990), flow angle of 45 degree is the most efficient angle through the research which measured flow angle by steady-state experiment. It is predicted that OCV A, SCV B and C in Fig. 4 contribute to improve in-cylinder combustion by minimizing the flow loss based on flow coefficient.

3.2 Fluid drift distribution within the engine cylinder

Figure 9 shows the ensemble mean velocity field

Table 2 Effects of OCV and SCV configuration on calculated Ricardo swirl ratio

	RS
baseline	2.22
OCV A	2.36
SCV B	2.52
SCV C	2.41
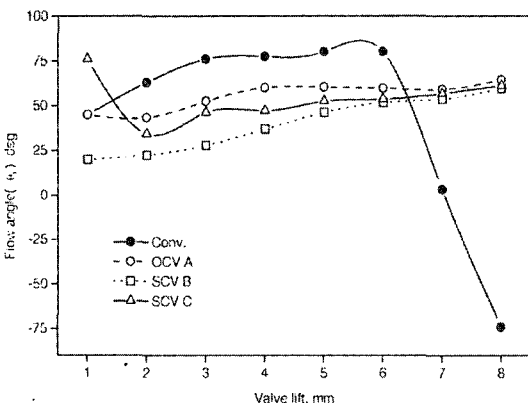
Fig. 8 Effects of OCV and SCV configuration on flow angle

(a) L=2 mm　　　　(b) L=4 mm

(c) L=6 mm　　　　(d) L=8 mm
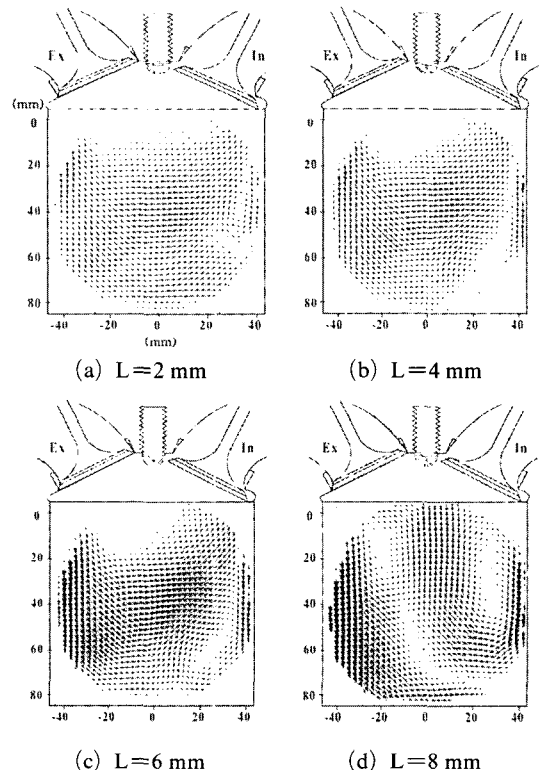
Fig. 9 The ensemble averaged velocity field of baseline engine

obtained by using cross-correlational PIV on the digitally-processed raw images. 1020 raw images were taken and 510 velocity fields were obtained. The four images in fig. 9 represent instances of velocity fields where the OCV or SCV was not attached to the baseline engine, with 2 mm valve lift increasing from 2 mm to 8 mm. Fig. 10 shows flow fields where the velocity vectors have been streamlined in order to more closely examine the direction of the velocity vectors. This was done by ensemble averaging the 510 instantaneous velocity fields. It can be observed that, under low valve lift conditions, the counter-clockwise rotational flow tumble flow beneath the exhaust port is larger than the clockwise rotational backward tumble flow beneath the intake port. The tumble flows are the result of intake flows turning into rotational flow due to the design of the valves and the combustion chamber. The intake flow either hits into or follows the contours of the cylinder
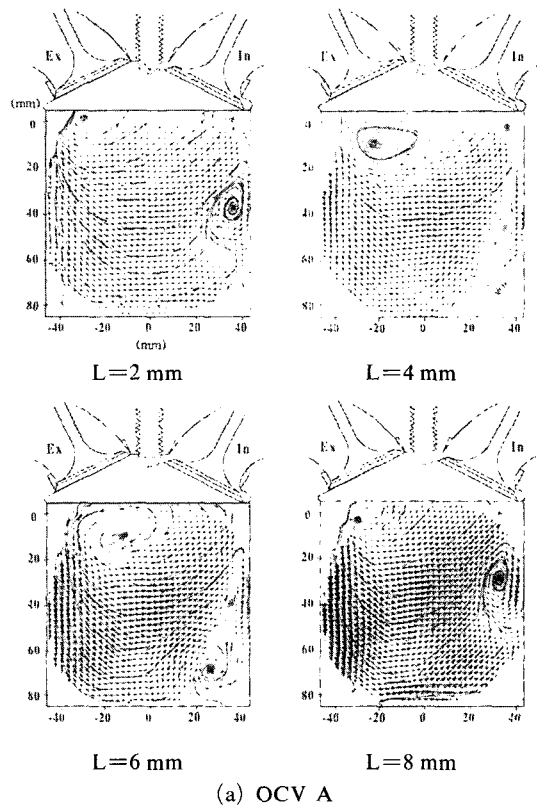
walls, turning into rotational flow. Also, it can clearly be observed that a vortex is created in the lower of intake valve, central part of the cylinder as the clockwise rotational flow backward tumble comes down the right-hand cylinder wall. As the valve lift is increased, the backward tumble is also intensified, and three vortices are created at maximum lift.

3.3 In-cylinder flow characteristics with addition of OCV and SCV

Fig. 11 shows the velocity vectors of in-cylinder tumble formation and flow characteristics in the stage of intake stroke when a OCV or SCV is attached to the intake port. The OCV or SCV adds a swirl component to the tumble flow. The OCV or SCV configuration was identical to that of Fig. 4, which were selected via steady-state flow experiments. Fig. 11 shows the creation of

(a) L=2 mm   (b) L=4 mm

(c) L=6 mm   (d) L=8 mm
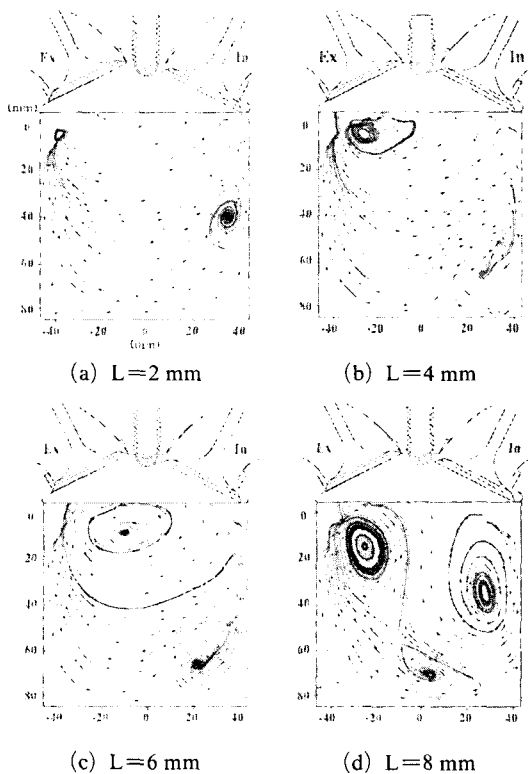
Fig. 10 The streamlines from ensemble averaged velocity field (Baseline engine)

L=2 mm   L=4 mm

L=6 mm   L=8 mm

(a) OCV A

Fig. 11 Ensemble averaged velocity field and streamlines

L=2 mm   L=4 mm

L=6 mm   L=8 mm

(b) SCV B

L=2 mm   L=8 mm
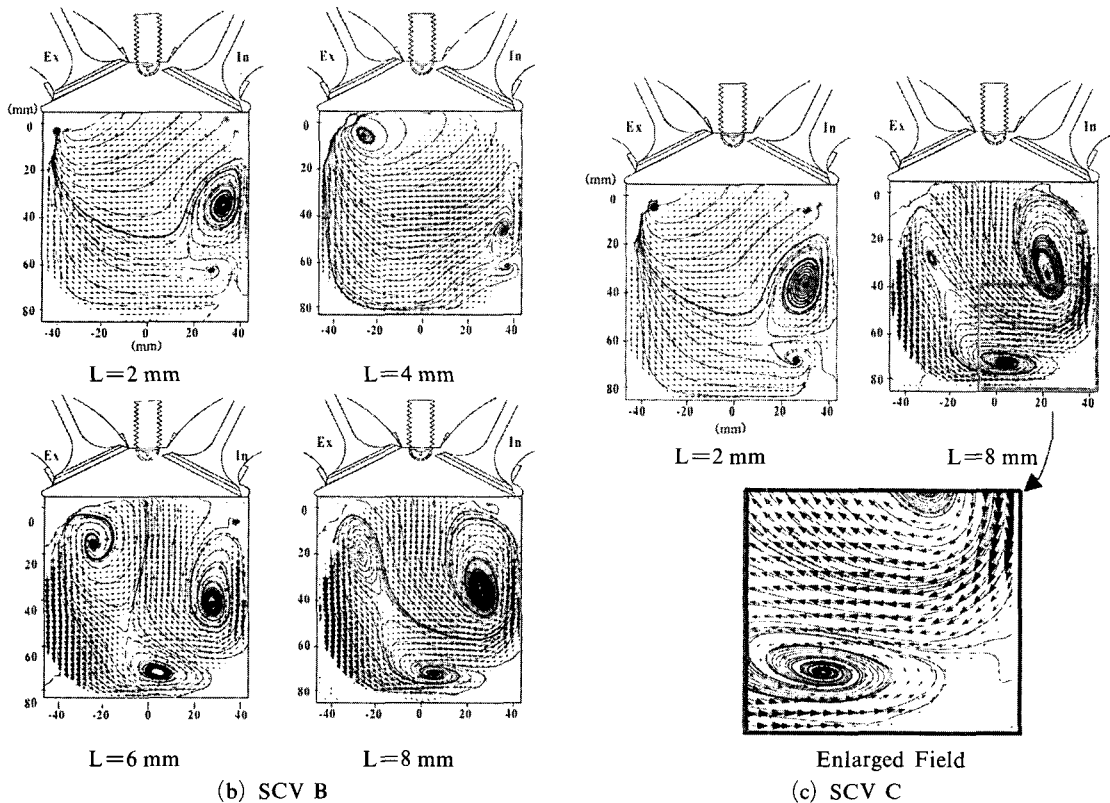
Enlarged Field

(c) SCV C

Fig. 11   Ensemble averaged velocity field and streamlines

flow fields when the valve lift was at 2~8 mm. The six flow visualizations show the flow fields depending on valve lift and OCV or SCV configuration. In the case of Fig. 11(a), a intensity of counter-clockwise tumble flow with the maximum velocity of 7.2 m/s throughout valve lift prevents the creation of the vortex that was observed in the lower, central part of the baseline engine cylinder. It can also be observed that the flow is guided towards the upper, right-hand side of the cylinder. Furthermore, it can be observed that a backward tumble flow with the maximum velocity of 5.1 m/s is created on the right-hand cylinder wall, but it is relatively small when compared to the other patterns. In Fig. 11(b), (c), it can be seen that B and C valve are both intense about both tumble flow and backward tumble flow. These intensity flows collide with the flow on both cylinder wall sides, and combined with the rotating swirl flow, creating a sort of friction that allows the flow characteristics of the inclined

tumble because the central direction is changed. Therefore, installation of OCV or SCV brings decrement in mean gas velocity, rectification of flow field but increases vortex component and contribution to lean burn as Lee's study.(Lee et al., 1998)

3.4 In-cylinder distribution of mean kinetic energy and turbulent kinetic energy

Instantaneous velocity, u_i, is a physically meaningful value of turbulence velocity, and can be broken down into mean velocity, U_i and fluctuation velocity, u_i'.

$$u_i = U_i + u_i' \qquad v_i = V_i + v_i' \qquad (3)$$

Mean velocity, U_i, indicate the average of time and the equation is as follows :

$$U_i = \lim_{T \to \infty} \frac{1}{T} \int_{t_0}^{t_0+T} u_i dt \qquad (4)$$
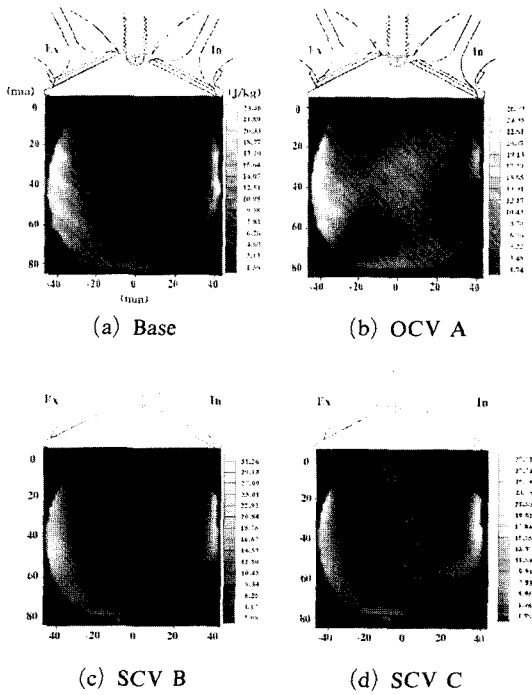
and the fluctuation intensities of turbulence are

(a) Base   (b) OCV A

(c) SCV B   (d) SCV C

Fig. 12 Mean kinetic energy distribution in cylinder (L=8 mm)

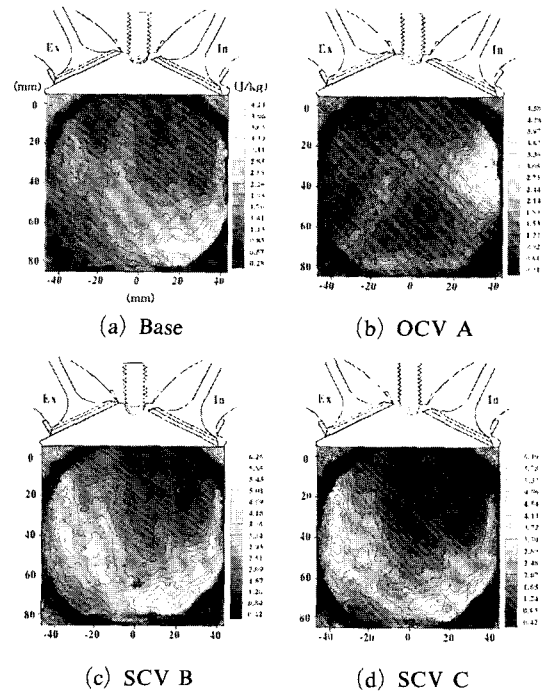(a) Base   (b) OCV A

(c) SCV B   (d) SCV C

Fig. 13 Turbulent kinetic energy distribution in cylinder (L=8 mm)

represented by $\sqrt{\overline{u'^2}}$, $\sqrt{\overline{v'^2}}$.

Figure 12 represents the distribution of mean kinetic energy by average velocity, and Fig. 13 represents the distribution of turbulent kinetic energy by in-cylinder fluctuation velocity. In Fig. 12, in-cylinder kinetic energy is more concentrated near cylinder wall than in the center. In case of adapting OCV or SCV, its spatial mean kinetic energy was larger than baseline engine because of the maximum flow velocity. but integral result of all visual area is relatively low in Fig. 14.

Figure 14 shows that the mean kinetic energy measured by using integral calculus processing of all visual fields 510 instances of velocity fields with valve lift from 2 to 8 mm by 2 mm interval were averaged. In a respect of mean kinetic energy, the baseline engine has higher value compared to the engine attached OCV A, SCV B and C throughout valve lift as 3.54, 3.44, 3.75 J/kg for 8 mm valve lift respectively. This result can be supposed that the intake air decreased when attaching OCV or SCV because of increased intake
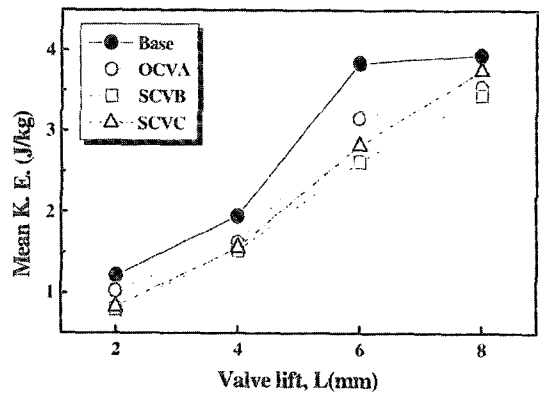

Fig. 14 Comparison of mean kinetic energy according to valve lift

air resistance. And it can be recognized that the result appears high in order of OCV A, SCV C, B according to OCV or SCV shape. It can be assumed that there is connection between the intake air and the valve open ratio. A remarkable thing is that the mean kinetic energy of valve B and C is increased lineally according to rising valve lift. On the other hand, valve C that has low

open ratio shows higher value than valve A that has high open ratio in maximum valve lift respectively. It can be treated with the effect by the rising of fluctuation component due to increasing flow velocity.

Figure 13 shows distribution of turbulent kinetic energy by fluctuation velocity. It is inspected that the engine with intense swirl flow has fluctuation component which spreads extensively to the center from cylinder wall in comparison with baseline engine and higher fluctuation at the lower part than one at the upper part in cylinder. It is inspected that intense turbulent kinetic energy appears at the position where swirl occurs. Therefore, the rise of fluctuation component will be contributed to combustion stabilization. As a result, turbulence has scaled down by piston compression effect.

Figure 15 compares Turbulent kinetic energy of baseline engine with the engine attached OCV or SCV throughout valve lift from 2 mm to 8 mm by 2 mm interval. The turbulent kinetic energy of fluctuation velocity was calculated by using integral calculus processing over all visual fields as mean kinetic energy is calculated above. Aspects of the turbulent kinetic energy of fluctuation velocity, the engine attached OCV A, SCV B and C by adding swirl flow was higher than baseline engine according to rising valve lift as 1.81, 2.16, 2.11 J/kg for 8mm valve lift respectively. Thus, this result is different from the mean kinetic energy. As Furuno's study (Furuno et al., 1990),
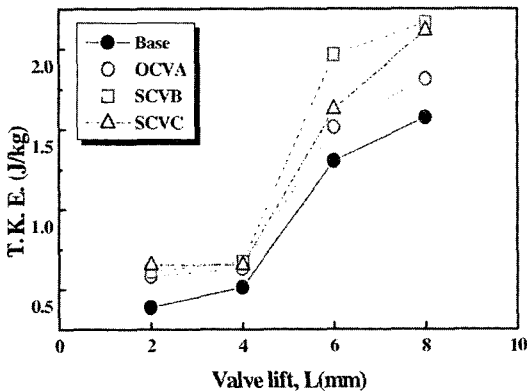
turbulent kinetic energy of SCV B, C which is close to flow angle of 45 degree have wider increase according to rising valve lift. Turbulent kinetic energy tends to increase with OCV or SCV installed, as a result of reinforcement of swirl flow according to flow of inclination tumble and finally improve lean burn (Bae et al., 1999). And it is in accord with Urushihara's study which deals various SCVs to improve combustion by reinforcing flow field created in combustion chamber, and revealed that it is more efficient to make the turbulent kinetic energy to reinforce swirl flow (Urushihara et al., 1995).

3.5 In-cylinder distribution of Reynolds shear stress

Figures 16 and 18 show the distribution of turbulent reynolds shear stress ($\overline{u'v'}$) from mean velocity field. The turbulent shear stress is generated by interaction of the turbulent component, u, and the horizontal gradient of intense vertical velocity on shear layer, and it means the kinetic transfer in flow field and the direction of
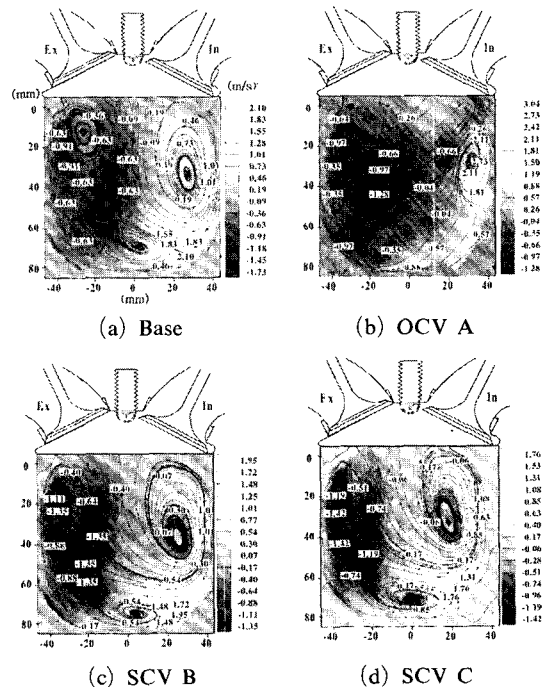

(a) Base   (b) OCV A

(c) SCV B   (d) SCV C

Fig. 16 Reynolds shear stress distribution in cylinder (L=8 mm)

Fig. 15 Comparison of turbulent kinetic energy according to valve lift

fluctuation component in turbulent flow. In the case of baseline engine, it is observed that turbulent shear stress by collision of flow is represented in right side wall neighborhood and lower part. Aspects of the turbulent kinetic energy, it is generated actively in right side wall neighborhood and lower part.

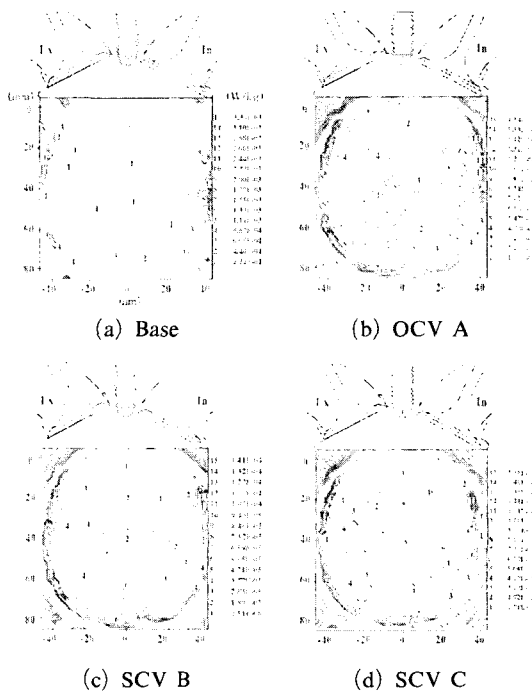In the case of SCV B, C, a part of tumble flow

(a) Base

(b) OCV A

(c) SCV B

(d) SCV C

Fig. 17 Dissipation energy distribution in cylinder (L=8 mm)
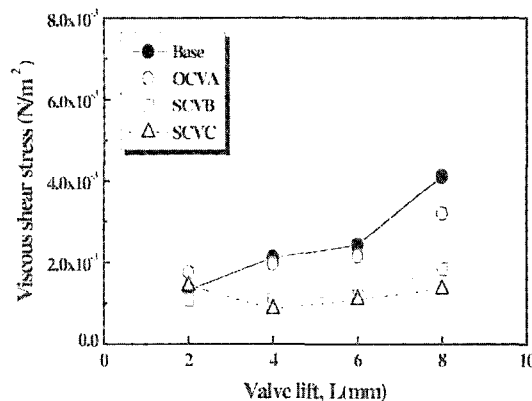

Fig. 18 Comparison of viscous shear stress according to valve lift

collide with cylinder upper part left side wall and it generated intensive vorticity, thus it shows the intense turbulent shear stress. Moreover, like baseline engine, the maximum shear stress is represented at the spot where being swept away after crashing tumble flow coming down from left wall and crashing piston crown before rising, and backward tumble shifting to right wall. Therefore, it is considered that turbulent generation is in active in this spot. Turbulent stress can be recognized as small amount of output.

3.6 In-cylinder distribution of energy dissipation

Fig. 17 shows the in-cylinder dissipation energy distribution for the baseline and OCV or SCV-attached engines at valve lift of 8 mm, in order to find the energy distribution of the flow allowing the grasping of energy destroy and to find energy conservation. Energy dissipation, D, was defined as follows, where the dissipation is the integral of the entire in-cylinder flow field.

$$D = \mu \left[2 \left(\frac{\partial u}{\partial x} \right)^2 + 2 \left(\frac{\partial v}{\partial y} \right)^2 + \left(\frac{\partial v}{\partial x} + \frac{\partial u}{\partial y} \right)^2 \right] \quad (5)$$

Above equation is the viscosity coefficient of the fluid ; x, y are the coordinate axes ; and u, v represent the flow velocity in the x and y direction, respectively. Energy dissipation is greater as 9.052×10^{-4} W/kg in the baseline engine than in the OCV A, SCV B and C engines as 4.1567, 2.896 and 2.785×10^{-4} W/kg for 8 mm valve lift respectively, and there is considerable energy destroy as the flow crashes into the cylinder walls. The energy dissipation rate is low for the lower zone of the baseline engine ; however, for the OCV or SCV-fitted engines, there is a great deal of energy destroy due to the collision of 1) the backward tumble that flows downward from the right-hand cylinder wall, and 2) the downward flow from the left-hand cylinder wall. These effects are minimized as the flows rise towards the top of the cylinder and become stable. Fig. 19 shows the comparison of dissipation energy according to valve lift. Energy dissipation greatly increases with increasing valve lift for the baseline engine. Of the OCV or SCV configurations,
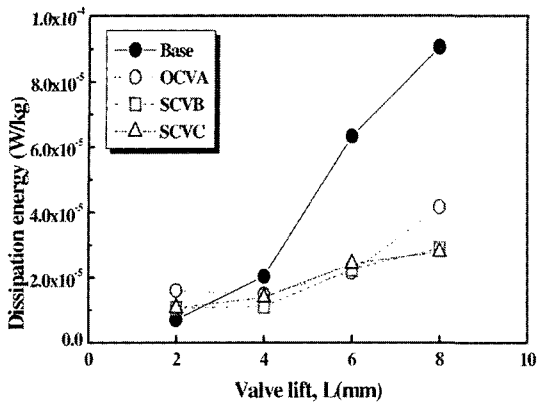
Fig. 19 Comparison of dissipation energy according to valve lift

valves B and C show the least dissipation which means that these configurations are best for energy conservation.

4. Conclusions

This paper studied the flow aspects of in-cylinder turbulent flow fields of a 2-valve pentroof gasoline engine. The tumble flow that is formed at the port during intake, and changes effected upon such a flow using a OCV or SCV, were analyzed using a steady-state flow experimental apparatus and 2-frame cross-correlation PIV technique. The following conclusions were obtained after quantitatively and qualitatively analyzing the turbulent characteristics due to changes in valve lift and OCV or SCV configurations.

(1) From the flow field of the baseline engine with varying valve lifts between 2 mm and 8 mm, it was visually confirmed that at low lifts tumble flows were dominant over backward tumble. Increase in valve lift resulted not only in increases of tumble flow but also in increases of backward tumble flow ; and at the maximum valve lift, friction of wall and flow collisions led to the creation of three large vortices.

(2) With the addition of a OCV or SCV, the flow characteristics changed according to the open ratio and configuration of the OCV or SCV. For valve OCV A, the tumble flow was strong as the maxi-　mum velocity of 7.2 m/s for all valve

lifts. SCV B and C had similarly strong tumble flows, plus strong backward tumble as the maximum velocity of 5.1 m/s ; the collision between these two flows, in addition to the swirl flow affects the central direction of the entire flow, creating inclined tumbles.

(3) The mean kinetic energy was lower because of the intake air decreased when attaching OCV A, SCV B and C by increasing intake air resistance as 3.54, 3.44, 3.75 J/kg for 8 mm valve lift respectively. Otherwise, aspect of the turbulent kinetic energy, the engine attached OCV A, SCV B and C by adding swirl flow was higher than baseline engine according to rising valve lift as 1.81, 2.16, 2.11 J/kg for 8 mm valve lift respectively. Therefore, the rise of fluctuation component will be contributed to combustion stabilization. As a result, turbulence has scaled down by piston compression effect.

(4) Energy dissipation was greater as 9.052-4 W/kg in the baseline engine than in the OCV A, B and C engines as 4.1567, 2.896 and 2.785-4 W/kg for 8 mm valve lift respectively, and a large degree of energy destroy caused by the flow collided against the cylinder walls. In the lower part of the cylinder, the dissipation rate was low for the baseline engine, but great in the OCV or SCV engine due to flow collisions. Based on the results that of all the OCV or SCV configurations, SCV B and C have the lowest energy dissipation for all valve lifts, it is believed these two configurations are the best for energy conservation.

References

Arcoumanis, C., Hu, Z. and Whitelaw, J. H., 1993, "Steady Flow Characterization of Tumble Generation Four-Valve Cylinder Heads," *Mech Processing Instn Mech Eng.*, Vol. 207, pp. 1~9.

Bae, C. S., Lee, J. H., Oh, S. M., Kang, K. Y., 1999, "The Effects of Tumble and Swirl Flows on the Flame Propagation in a 4-valve SI Engine," *Jounal of KSAE*, 7, 2, pp. 50~58.

Furuno, S., Iguchi, S., Oishi, K. and Inoue, T., 1990, "The Effects of Inclination Angle of Swirl axis on Turbulence Characteristics in a

Lean Burn Engine with SCV," COMODIA 90, pp. 437–442.

Hacohen, J., Beltmont, M. R. and Ashcroft, S. J., 1994, "Flame Speeds in a Spark Ignition Engine," *SAE Paper* No. 942050.

Lee, J. H. and Farrell, P. V., 1993, "Intake Valve Measurement of an in Engine Using Particle Image Velocimetry," *SAE Paper* No. 930480, pp. 629~645.

Lee, K. H., Lee, C. S., Lee, H. G., Chun, M. S. and Joo, Y. C., 1998, "Spatial Analysis of Turbulent Flow in Combustion Chamber using High Resolution Dual Color PIV," *Jounal of KSAE*, 6, 6, pp. 132~141.

Lee, K. H., Lee, C. S., Lee, H. G., Chon, M. S. and Joo, Y. C., 1998, "Spatial Analysis of Turbulent Flow in Combustion Chamber using High Resolution Dual Color PIV," *Journal of KSAE*, 6, 6, pp. 132~141.

Melling, A., 1997, "Tracer Particles and Seeding for Particle Image Velocimetry," *Meas. Sci. Technol.*, Vol. 8, pp. 1406~1416.

Ronnback, M. et al., 1991, "Study of Induction Tumble by Particle Tracking Velocimetry in a 4-Valve Engine," *SAE Paper* No. 912376, pp. 25~32.

Sung, J. Y. and Lee, I. S., 2003, "Optimal Flow Control of Ceiling Type Indoor Unit by PIV Measurements," *Transactions of the KSME*, B, Vol. 27, No. 8, pp. 1042~1050.

Urushihara, T., Murayama, T., Takagi Y. and Lee K. H., 1995, "Turbulence and Cycle-by-cycle Variation of Mean Velocity Generated by Swirl and Tumble Flow and Their Effects on Combustion," *SAE Paper* No. 950813.

Woo, Y. W. and Lee, C. S., 2002, "A Study on the Spray Characteristics for a Gasoline Direct Injector by Using Entropy Analysis and PIV Methods," *Transactions of the KSME*, B, Vol. 26, No. 7, pp. 1047~1054.